Journal of Applied Fluid Mechanics, Vol. 15, No. 3, pp. 843-855, 2022.
Available online at www.jafmonline.net, ISSN 1735-3572, EISSN 1735-3645.
https://doi.org/10.47176/jafm.15.03.33280

Modeling of Bubbly Flow using a Combined Volume of Fluid and Discrete Bubble Model: Investigation on Interphase Forces

H. Yang, J. Xue, L. Li, X. Li†, P. Lin and Z. Zhu

National-Provincial Joint Engineering Laboratory for Fluid Transmission System Technology, Zhejiang Sci-Tech University, Hangzhou, Zhejiang, 310018, China

†*Corresponding Author Email: lixiaojun530@163.com*

(Received August 13, 2021; accepted December 18, 2021)

ABSTRACT

The gas-liquid two-phase flow with interfacial behaviors and bubble-liquid interactions is widely encountered in industrial processes such as that in gas-liquid reactors. The complicated phase structure makes it difficult to be modeled. The present work proposes a multi-scale mathematical model to simulate the bubbly flow in a square column. The volume of fluid (VOF) method is applied to treat the separated interface, and the discrete bubble model (DBM) is incorporated to handle the dynamics of dispersed bubbles. The hybrid model is validated against the benchmark experimental data to study the accuracy and suitability of the modeling framework for bubbly flows. And the influence of interphase forces on bubbly flow patterns and velocity profiles is investigated. It is found that the employment of both pressure gradient force and Ishii-Zuber drag model provides fairly good agreements with experimental data for velocity profiles.

Keywords: Gas-liquid two-phase flow; Multi-scale model; Volume of fluid; Discrete bubble model.

NOMENCLATURE

a	amplitude
A	area
b	value of the actual collision parameter
b_{cri}	criteria impact parameter
C_D	drag force coefficient
C_{VM}	virtual mass force coefficient
D	diameter
d	distance
$\mathbf{F}_G$	gravity
$\mathbf{F}_L$	lift force
$\mathbf{F}_P$	bubble force acting on liquids
$\mathbf{F}_b$	surface tension
$\mathbf{F}_{PG}$	pressure gradient force
$\mathbf{F}_S$	Saffman lift force
$\mathbf{F}_{VM}$	virtual mass force
$\mathbf{g}$	gravitational acceleration
k	kinetic energy
K	ratio of the total energy in distortion
m	mass of individual bubble
n	number of collisions
p	pressure
P	probability of collision
Q	gas flow rate
r	bubble radii
Re	Reynolds number
S	rate-of-strain tensor
T	integral time scale
t	time
$\mathbf{u}$	liquid velocity
$\mathbf{v}$	bubble velocity
$\mathbf{v}_T$	terminal bubble velocity
V_{cell}	cell volume
We_c	collisional Weber number
α	volume fraction
ρ	density
σ	surface-tension coefficient
μ	viscosity
μ_t	turbulent viscosity
κ	curvature of free surface
δ_{ij}	dirac function
λ	expected number of collisions
ω	specific dissipation rate

1. INTRODUCTION

In many industrial processes, the gas-liquid two-phase flow is widely found, such as bubble column reactor, chemical material synthesis, waste water treatment and fuel synthesis (Liu and Hu 2004). The process is accompanied by complex flow patterns and phase interactions, which is necessary to obtain detailed parameters to

reveal the characteristics of the flow field inside the reactor and the motion of bubbles. For large-scale chemical reactors, there are great limitations to obtain operating parameters through experiments. Computational fluid dynamics (CFD) (Jiang *et al*. 2016; Wang and Wang 2007) is proven to be able to simulate and analyze fluid dynamics problems, and to provide data that cannot be obtained by traditional experiments, both in time and space. Therefore, CFD is increasingly used in the research of industrial gas-liquid reactors. However, due to the poor versatility of mathematical closures in CFD and the limits in model capabilities, the simulation of bubble column reactors still needs a lot of research. Only through experimental data to verify the mathematical closure in CFD can make it clearer about the scope of application of mathematical closures. In addition, due to the complicated interactions, it is very difficult to predict bubble behaviors and mixed flow phenomena in the bubble column reactor.

In recent years, Euler-Euler (E-E) and Euler-Lagrange (E-L) methods are usually applied in simulation of bubble column reactors. The E-E method treats each phase as a continuum, and the equations of mass and momentum of each phase is solved to describe the macroscopic distribution of the phase in space. This method does not require high computational capability and is unable to obtain the information of a single bubble, so it is difficult to simulate the coalescence or break-up of bubbles in the actual process (Chahed *et al*. 2003; Passalacqua and Fox 2011; Pfleger *et al*. 1999; Zhou 2010). Matiazzo *et al*. (2020) used the Euler-Euler method to simulate the gas-liquid flow in the bubble column, and investigated the influence of different drag closures, breakup and coalescence models on the model prediction. As an alternative, in the E-L method, the discrete phase can be directly tracked by the Lagrangian method, so the size and distribution of bubbles can be accurately simulated. In this method, both the bubble-liquid interaction and bubble-bubble interaction are considered, so that the motion of discrete phase can be understood more deeply. In the 1990s, Hoomans *et al.* (1996) established a discrete particle model to investigate gas-fluidized beds, using a hard sphere collision model to explain the movement of bubbles. Delnoij *et al.* (1997) proposed a gas-liquid two-phase flow model based on E-L model which described the two-dimensional movement of bubbles in the bubble column. The effect of aggregation and breakage of bubbles on bubbly flow may be significant. Therefore, more and more researches have been done to study the coalescence and break-up model in the E-L method. van den Hengel *et al*. (2005) added a bubble coalescence and break-up model on basis of the DBM established by Delnoij *et al*. (1997). Bourloutski and Sommerfeld (2004) introduced a random Lagrangian bubble collision model without considering bubble break-up. Darmana *et al*. (2006) reported a parallel algorithm considering four-way coupling, the coalescence and collision between bubbles were accounted. Bokkers *et al*. (2006) adopted the pseudo-fluid algorithm for emulsion phase, and the bubbles were calculated by Lagrangian method to explore the influence of DBM and closure relations on bubble coalescence and break-up in fluidized beds.

DBM provides a feasible solution for the simulation of small-scale bubbles, but when there are large-scale continuous interfaces in the system, a single DBM is not applicable. In response to this problem, a hybrid model is proposed, that applies the volume of fluid (VOF) method to capture the large-scale interface while using DBM to simulate bubbles at a small scale without considering the boundary (Li and Li 2018; Li *et al*. 2017; Liu *et al*. 2014; Ma *et al*. 2012; Xu *et al*. 2013). The VOF method first proposed by Hirt and Nichols (1981) is one of the most commonly used methods for interface capturing. It has good mass conservation characteristics and can calculate the geometric properties of the interface accurately (Zhang *et al*. 2012). Cloete *et al*. (2013) coupled the VOF and DPM to evaluate the influence of various design and operating variables on the gas-liquid flow in the ladle. Jain *et al*. (2014) proposed a VOF-DBM method to simulate the rise of bubbles in water and the wave behavior of free surface. Olsen and Skjetne (2016) combined the VOF and DBM methods to solve the underwater bubble motion considering the dissolution. Li *et al*. (2020) proposed a VOF-DBM model with considering the bubble aggregation and the discrete-continuum transition to predict the multiphase flow in a gas-stirred ladle.

In summary, various multi-scale models are utilized to simulate phenomena that occur at different scales. In order to better predict the bubble flow characteristics in bubble column reactors, it is still necessary to investigate the interaction between bubble and liquid. The objective of this work is to propose a multi-scale model to capture the large-scale continuous interface while simulating the behavior of small-scale bubbles and investigate the effect of different interphase forces.

2. MATHEMATICAL MODEL

In this work, VOF is utilized to deal with the free surface of liquid which is regarded as a continuous phase, and DBM is proposed to investigate the motion of discrete bubbles.

2.1 Volume of Fluid Method

The continuous interface tracking in VOF method is based on the solution of one momentum equation for the gas and liquid phases, and an equation is used for the volume fraction of one phase. Gas and liquid phases are considered as incompressible fluids. The equation of volume fraction is given by

$$\frac{\partial \alpha}{\partial t}+\mathbf{u}\cdot\nabla\alpha=0 \tag{1}$$

where α, $\mathbf{u}$ respectively represent the volume fraction and velocity. The primary phase is not

solved by the volume equation, but is instead calculated from the relation:

$$\alpha_p = 1-\alpha \tag{2}$$

The momentum equation for the gas-liquid mixture is based on the following equation:

$$\rho\left(\frac{\partial(\mathbf{u})}{\partial t}+\nabla\cdot(\mathbf{uu})\right)=-\nabla p+\nabla\left(\mu\left(\nabla\mathbf{u}+\nabla\mathbf{u}^T\right)\right)+\rho\mathbf{g}+\mathbf{F}_b+\mathbf{F}_p \tag{3}$$

where **F**p represents bubble-liquid interface coupling relations, ρ and μ represent the density and viscosity of the mixture that are written as:

$$\rho=\alpha\rho_l+(1-\alpha)\rho_b \tag{4}$$

$$\mu=\alpha\mu_l+(1-\alpha)\mu_b \tag{5}$$

The continuum-surface-force model is utilized to evaluate the surface tension (Brackbill *et al.* 1992) as:

$$\mathbf{F}_b=\sigma\kappa\nabla\alpha \tag{6}$$

where σ represents the surface-tension coefficient and κ represents the surface curvature which calculated as follows:

$$\kappa=-\nabla\cdot\left(\nabla\alpha/|\nabla\alpha|\right) \tag{7}$$

2.2 Turbulence Model

Shear stress transfer (SST) *k*-ω model is a turbulence model proposed by the Menter (1994) on the basis of *k*-ε model and *k*-ω model. The model uses the *k*-ε model in the fully developed area and *k*-ω model near the wall to improve the prediction accuracy and reliability of the free flow near wall. The equations of turbulent kinetic energy *k* and specific dissipation rate ω are given by:

$$\frac{\partial\rho\alpha_l k}{\partial t}+\frac{\partial\rho\alpha_l u_j k}{\partial x_j}=\alpha_l P-\alpha_l\beta^*\rho k\omega+\frac{\partial}{\partial x_j}\left[\alpha_l(\mu+\sigma_k\mu_t)\frac{\partial k}{\partial x_j}\right] \tag{8}$$

$$\frac{\partial\rho\alpha_l\omega}{\partial t}+\frac{\partial\rho\alpha_l u_j\omega}{\partial x_i}=\alpha_l\frac{\gamma}{\nu_t}P-\alpha_l\beta\rho\omega^2$$

$$+\frac{\partial}{\partial x_j}\left[\alpha_l(\mu+\sigma_\omega\mu_t)\frac{\partial\omega}{\partial x_j}\right]+2(1-F_1)\frac{\rho\alpha_l\sigma_{\omega 2}}{\omega}\frac{\partial k}{\partial x_j}\frac{\partial\omega}{\partial x_j} \tag{9}$$

where production term $P=\tau_{ij}\frac{\partial ui}{\partial x_j}$, turbulent stress and rate-of-strain tensor are given by:

$$\tau_{ij}=\mu_t\left(2S_{ij}+\frac{2}{3}\frac{\partial u_k}{\partial x_k}\delta_{ij}\right)-\frac{2}{3}\rho\delta_{ij} \tag{10}$$

$$S_{ij}=\frac{1}{2}\left(\frac{\partial u_i}{\partial x_j}+\frac{\partial u_j}{\partial x_i}\right) \tag{11}$$

The eddy viscosity is calculated as follows:

$$\mu_t=\frac{\rho\alpha_l k}{max\left(\alpha_l\omega, SF_2\right)} \tag{12}$$

where *S* represents a modulus of the rate-of-strain tensor which is written as $\sqrt{2S_{ij}S_{ij}}$.

2.3 Discrete Bubble Model (DBM)

The motion of each individual bubble is obtained by solving Newton's second law. A two-way coupling method is applied between continuous phase and bubbles. All the forces exerted on a bubble is summed up. Then the equations for an incompressible bubble are described as follows:

$$\rho_b V_b\frac{d\mathbf{v}}{dt}=\sum\mathbf{F} \tag{13}$$

$$\sum\mathbf{F}=\mathbf{F}_G+\mathbf{F}_{PG}+\mathbf{F}_D+\mathbf{F}_S+\mathbf{F}_{VM} \tag{14}$$

where ρ_b, V_b, and **v** represent the bubble density, bubble volume and bubble velocity respectively. The net force $\sum\mathbf{F}$ is the resultant force on bubbles, and the terms on the right-hand side of Eq. (14) represent the gravity, pressure gradient force, drag force, Saffman lift force and virtual mass force, respectively.

The term of $\mathbf{F}_D$ describes drag force acting on bubbles, which is written as:

$$\mathbf{F}_D=-\frac{3}{4}\alpha\rho_l\frac{C_D}{D_b}|\mathbf{v}-\mathbf{u}|(\mathbf{v}-\mathbf{u}) \tag{15}$$

Ishii and Zuber (1979) gave the following expression for the drag coefficient C_D:

$$C_D=\frac{2}{3}\sqrt{Eö} \tag{16}$$

The drag model plays a significant role in the phase interaction, so it is selected to investigate the interphase interaction in the bubble square column after comparing other drag models proposed by Morsi and Alexander (1972) and Grace and Weber (1978).

The drag coefficient C_D proposed by Morsi and Alexander (1972) can be expressed as:

$$C_D=C_1+\frac{C_2}{Re}+\frac{C_3}{Re^2} \tag{17}$$

Grace and Weber (1978) gave the following expression for the drag coefficient C_D:

$$C_D=max\left\{\frac{24}{Re}\left(1+0.15\,Re^{0.687}\right), min\left(\frac{8}{3}, \frac{4gd_b\Delta\rho}{3\mathbf{v}_T^{\,2}\rho_l}\right)\right\} \tag{18}$$

The reason for selecting the drag model proposed by Ishii and Zuber is discussed in section 4.1.

Note that the Saffman lift force investigated in this work can be obtained from Li and Ahmadi (1992). The expression of the Saffman lift force can be written as the following, which is provided by Saffman (1965):

$$\mathbf{F}_s = \frac{2K\mathbf{v}^{1/2}\rho_l d_{ij}}{\rho_b D_b \left(d_{lk}d_{kl}\right)^{1/4}}\left(\mathbf{u}\text{-}\mathbf{v}\right) \tag{19}$$

The rest relevant forces include the gravity, virtual mass force and pressure gradient force, which can be expressed by the following equations:

$$\mathbf{F}_{\mathrm{G}} = \rho_b V_b \mathbf{g} \tag{20}$$

$$\mathbf{F}_{VM} = -\left(C_{VM}\rho_l V_b \frac{D\left(\mathbf{v}\text{-}\mathbf{u}\right)}{D\mathrm{t}} + C_{VM}\rho_l V_b\left(\mathbf{v}\text{-}\mathbf{u}\right)\cdot\nabla\mathbf{u}\right) \tag{21}$$

$$\mathbf{F}_{\mathrm{PG}} = -V_b\nabla p \tag{22}$$

where C_{VM} is the virtual mass coefficient and is equal to 0.5.

In the actual process, when the bubble reaches the liquid level, it will leave the gas-liquid interface to become part of the continuous gas phase. Therefore, when bubbles reach the gas-liquid interface ($\alpha > 0.5$), the bubble tracking stops. Gas volume fraction equation and current cell velocity equation can be described as：

$$\alpha = \alpha + V_b / V_{cell} \tag{23}$$

$$\mathbf{u} = \mathbf{u} + V_b\mathbf{v}/V_{cell} \tag{24}$$

2.3.1 Discrete Random Walk Model

The bubble diffusion caused by turbulence in the flow field can be predicted by a random walk model. This random tracking method can not only calculate the trajectory of particles effectively, but also consider the influence of turbulence on particle dispersion.

The concept of the integral time scale T is used to make a prediction of the particle dispersion, which is given by：

$$\mathrm{T} = \int_0^\infty \frac{u_p'\left(t\right)u_p'\left(t-\tau\right)}{\overline{u_p'^2}}d\tau \tag{25}$$

The integration time is directly proportional to the diffusion rate of particle, and a smaller value indicates less turbulent motion. The particle diffusivity is described as $\overline{ui'uj'}T$.

As for small “tracer” bubbles which move with the fluid, the integral time becomes the fluid Lagrangian integral time. For the *k-ω* model and its variants, the time scale $\mathrm{T_L}$ is expressed by the following equation:

$$T_L \approx 0.30\frac{k}{\varepsilon} \tag{26}$$

The random walk model considers the interaction between bubbles and discrete vortices of fluid (Gosman and Ioannides 1983). Each eddy is characterized by a random velocity fluctuation which follows a Gaussian distributed u' , v' , w' and a time scale τ.

For the *k-ω* model and its variants. When using the Reynolds stress model, the non-isotropy of the stress is included in the derivation of the velocity fluctuation:

$$u' = \varsigma\sqrt{\overline{u'^2}}\ , v' = \varsigma\sqrt{\overline{v'^2}}\ , w' = \varsigma\sqrt{\overline{w'^2}} \tag{27}$$

where ς represents a random number that is distributed normally, the characteristic lifetime of the eddy can be given by:

$$\tau_e = 2T_L \tag{28}$$

where T_L can be obtained from Eq. (26).

2.3.2 Coalescence Model

In the collision algorithm, there are $1/2N^2$ possible collision time to be calculated at each time step. Taking the bubble column reactor in this paper as an example, the simulation will produce innumerable bubbles, which will cause huge consumption of computing resources. Thus, the concept of parcels is proposed, which is a statistical representation of multiple individual bubbles.

Once the collision between two bubbles is determined, the algorithm will further determine the type of collision. The probability of results are calculated from a fit to experimental observations and the collisional Weber number (We_c).

$$We_c = \frac{\rho\mathbf{u}_{rel}^2\overline{D}}{\sigma} \tag{29}$$

where $\mathbf{u}_{\mathrm{rel}}$, $\overline{D}$ represent the relative velocity between two parcels and the arithmetic mean diameter of two parcels, respectively.

The probability of collision of two bubbles is derived from the point of view of the larger bubble, which identified with the number 1. The smaller bubble is identified with number 2. A collision will occur, if the center of the smaller bubble passes through a flat circle centered around the collector of area $\pi\left(r_1+r_2\right)^2$ perpendicular to the trajectory of the smaller bubble. The collision probability between the smaller bubble and collector is defined as:

$$P_1 = \frac{\pi\left(r_1+r_2\right)2\mathbf{v}_{rel}\Delta t}{V_{cell}} \tag{30}$$

where $\mathbf{v}_{rel}$ represents the relative velocity between two bubbles. It can be obtained from Eq. (31) that there are i_1 bubbles in the collector and i_2 bubbles in the smaller bubble parcels. The mean expected collision number of collectors is defined as follows:

$$\overline{n} = \frac{n_2\pi\left(r_1+r_2\right)2\mathbf{v}_{rel}\Delta t}{V_{cell}} \tag{31}$$

The probability distribution of the actual number of collisions underwent by the collector follows the Poisson distribution, which can be defined as:

$$P_{(n)} = e^{-\bar{n}} \frac{\bar{n}^n}{n!} \tag{32}$$

where n represents the collision number between bubbles and a collector. In this present work, the probability of bubble coalescence may be caused by the offset of the collector bubble center. According to O'Rourke (1981), the critical offset is given by:

$$b_{crit} = (r_1 + r_2)\sqrt{min\left(1.0, \frac{2.4f}{We_c}\right)} \tag{33}$$

where f represents a function of bubble size ratio, which is defined as $(r_1/r_2)^3 - 2.4(r_1/r_2)^2 + 2.7(r_1/r_2)$. b is a value of the actual parameter of collision, which can be defined as:

$$b = (r_1 + r_2)\sqrt{Y} \tag{34}$$

where Y represents a random number range in [0, 1). If $b < b_{crit}$, bubbles will coalescence. The properties of the coalesced bubbles can be obtained from the following equations：

$$m_1^{'} = m_1 + m_2 \tag{35}$$

$$m_1^{'}\mathbf{v}_1^{'} = m_1\mathbf{v}_1 + m_2\mathbf{v}_2 \tag{36}$$

Otherwise, a grazing collision takes place. The new bubble velocity is determined according to the conservation of momentum, which is given by:

$$\mathbf{v}_1^{'} = \frac{m_1\mathbf{v}_1 + m_2\mathbf{v}_2}{m_1 + m_2} + \frac{m_2(\mathbf{v}_1 - \mathbf{v}_2)}{m_1 + m_2}\left(\frac{b - b_{crit}}{r_1 + r_2 - b_{crit}}\right) \tag{37}$$

$$\mathbf{v}_2^{'} = \frac{m_1\mathbf{v}_1 + m_2\mathbf{v}_2}{m_1 + m_2} - \frac{m_2(\mathbf{v}_1 - \mathbf{v}_2)}{m_1 + m_2}\left(\frac{b - b_{crit}}{r_1 + r_2 - b_{crit}}\right) \tag{38}$$

where m_1 and m_2 are the masses of bubble 1 and bubble 2, respectively.

2.3.3 Break Up Model

In this study, we utilize a break-up model suitable for the condition with low Weber number. And bubbles will break only if the following equation is valid:

$$We_c + a > 1 \tag{39}$$

where a represents the amplitude of an undamped oscillation ($t_d \approx \infty$) for each bubble at time step n, which is defined as $\sqrt{(y^n - We_c)^2 + \left(\frac{(dy/dt)^n}{\omega}\right)^2}$. The breakup time is obtained under the assumption that the bubble oscillation is undamped for its first period. Thus, the breakup time is the smallest root greater than t^n of an undamped version:

$$We_c + a\cos\left[\omega\left(t - t^n\right) + \varphi\right] = 1 \tag{40}$$

where $\cos\phi = \frac{y^n - We_c}{a}$ and $\sin\phi = -\frac{(dy/dt)^n}{a\omega}$.

If $t_{bu} > t^{n+1}$, breakup can't take place. Then the next bubble will be calculated. On the contrary, if $t^n < t_{bu} < t^{n+1}$, the breakup will take place and the child bubble radius is expressed by the following equation:

$$r_{32} = \frac{r}{1 + \frac{8Ky^2}{20} + \frac{\rho_l r^3 (dy/dt)^2}{\sigma}\left(\frac{6K - 5}{120}\right)} \tag{41}$$

where K represents the ratio of the total energy in distortion.

3. NUMERICAL DETAILS

The geometry and mesh of computational domain of the square column are shown in Fig. 1. The cross section of the square column (W*D) is 0.15m*0.15m, and the height (H) is 0.5m (water level is at 0.45m). The black line in Fig. 1 indicates the measurement position which along the y direction at a height of 0.25m. More relevant simulation settings and detailed parameters can be found in Table 1. A gas distributor which has 49 pores with diameter of 1 mm is placed in the center of the bottom plane, and air is injected into the system at a superficial gas velocity of 4.9 mm/s. According to Deen's case (Deen *et al.* 2001), the initial bubble diameter is 4 mm.

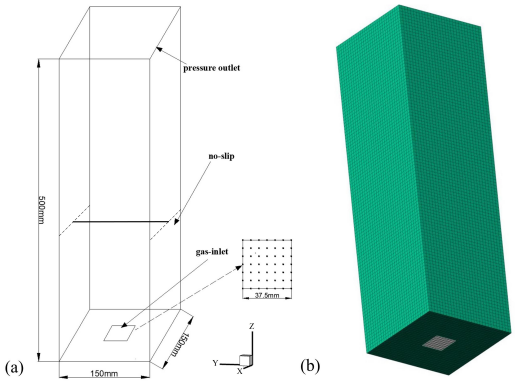

Fig. 1. (a) Geometry of the numerical domain, (b) Mesh of computational domain of the square column.

The number of cells in x, y and z directions for bubble column is 28, 28 and 100 respectively, which gives a total of 78400 cells. The boundary condition is defined at the inlet consists of 7×7 grids as follows:

Table 1. Simulation parameters.

Parameter	Value
Width (W)	150mm
Depth (D)	150mm
Height (H)	500mm
Water level (L)	450mm
Water density	998.2kg·m^{-3}
Water viscosity	1.0×10^{-3}kg·m^{-1}·s^{-1}
Superficial gas velocity	4.9mm·s^{-1}
Bubble density	1.2kg·m^{-3}
Initial bubble diameter	4mm

$$\mathbf{v}_{y,in} = \frac{\mathbf{v}_s W \times D}{A_{in}} \tag{42}$$

where $\mathbf{v}_s$ represents the superficial gas velocity. In the case, $W \times D$ equals to 0.0375 m×0.0375 m. The value of inlet velocity is 0.0784 m/s which is normal to the inlet. Pressure boundary is modelled at the outlet, while other boundaries are set as no-slip walls.

The Pressure-Implicit with Splitting of Operators (PISO) method is used for the pressure-velocity coupling while *k-ω* SST model is used for turbulence. For the discretization of the partial differential equations system, the least square cell based method is utilized. Second-order upwind is applied to the spatial discretization for momentum and geo-reconstruct schemes are adopted for the volume fraction. The total simulation time is 300s with a time step of 0.01s, and the first 20s is discarded due to unsteady flow filed. The numerical simulation is performed using the Fluent software. To simulate the behaviors of bubbles coming through the gas-liquid interface and transforming to the continuous gas. A user defined function (UDF) is implemented in the present work.

4. RESULTS AND DISCUSSION

Three stages of simulations are carried out in the present work. First, the performance of three different drag models, which are proposed by Ishii and Zuber (1979), Morsi and Alexander (1972) and Grace and Weber (1978), are evaluated to determine the appropriate one used for all further simulations. In section 4.2, the various single additional interphase forces including pressure gradient force, virtual mass force and Saffman lift force are considered. In section 4.3, the effect of two interphase forces based on the drag model is discussed, which indicates that another different single additional interphase force is added to the chosen model. The most suitable drag model and interphase force closures are used for simulation and the transient bubble flow characteristics are provided in section 4.4.

4.1 Effect of different drag closures

The drag force is a key factor that determines the interaction between phases and the velocity of bubbles. It can be decomposed into form drag and viscous resistance. The form drag is generated by the pressure difference around the moving bubbles in the liquid, and the viscous resistance is caused by the velocity gradient and viscous stress in the boundary layer. Three different drag closures including spherical, Grace and Ishii-Zuber models are chosen to investigate their applicability for drag closures. All numerical simulation parameters are the same except for the drag closure.

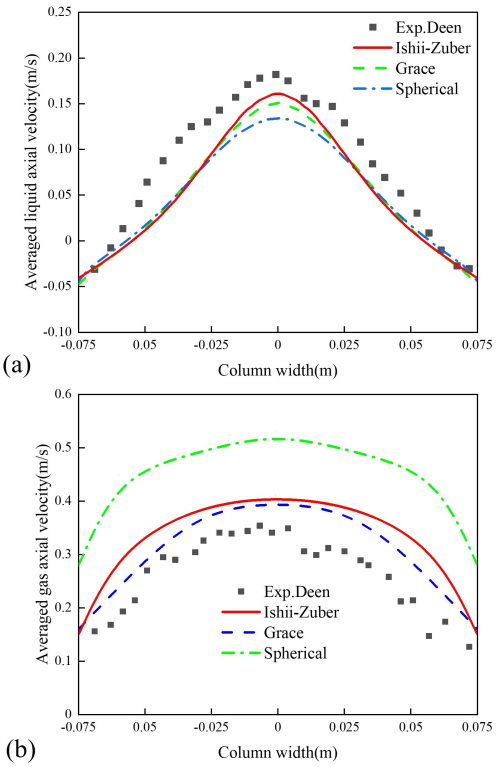

Fig. 2. Effect of different drag closures: (a) time-averaged axial liquid velocity at the height of 0.25m. (b) time-averaged axial gas velocity at the height of 0.25 m.

The effect of various drag models on mean axial liquid velocity and gas velocity are shown in Fig. 2 and the bubble distributions are shown in Fig. 3. The predicted results are compared with the experiment data from Deen *et al.* (2000). Both mean axial velocity profiles for liquid and gas at the positions of black line show that the maximum velocity is in the central part and the velocity decreases from center outwards. The circulation of the liquid phase drives the liquid upward in the central position and downward close to the walls. Therefore, the mean axial liquid velocity is the maximum near the center, and negative values appear near the wall. As for the mean axial liquid velocity, it is evident that three drag models exhibit a relative flat profile, which under-estimates the experimental data. The velocity profiles predicted by Ishii-Zuber model and spherical model are more accurate compared with the experimental value. On the contrary, there is an over-prediction of the mean axial gas velocity. Since the spherical

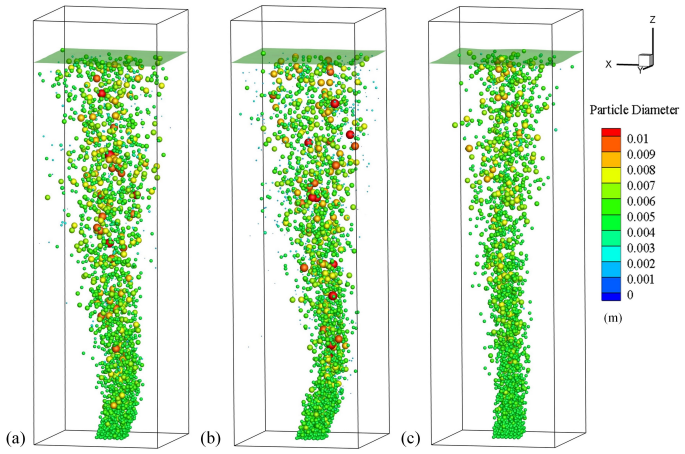

Fig. 3. Instant snapshots of the bubble plume and gas–liquid interface for the tested drag models: (a) Ishii-Zuber drag model (b) Grace drag model (c) spherical drag model.

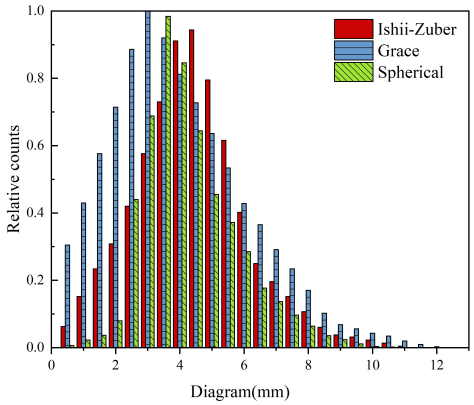

Fig. 4. Overall bubble size distribution for tested drag models.

drag model does not consider the energy dissipation of the discrete phase, thus it substantially over-estimates the gas velocity for all positions. It also can be seen from Fig. 3(c) that the bubble plume is more concentrated during the rising process due to the larger axial gas velocity. Drag models proposed by Ishii-Zuber and Grace predict the mean gas velocity profiles better compared to the spherical drag model.

As illustrated in Fig. 4. the bubble diameter distribution under the Ishii-Zuber model is closer to the normal distribution, that is, the peak value of bubble diagram is in the middle, and the values on both sides are roughly symmetrical. The coalescence and the breakup of bubbles are more obvious using the Grace model, because of that the relative counts of small bubbles and large bubbles are increased compared with the results using the other two drag models. On the contrary, the rate of bubble coalescence and breakup is the least using the Spherical model. In conclusion, the Ishii-Zuber drag model will be used for all further simulations. However, it is impossible to predict the velocity profiles accurately only by considering the drag force. Thus, the effects of additional interphase

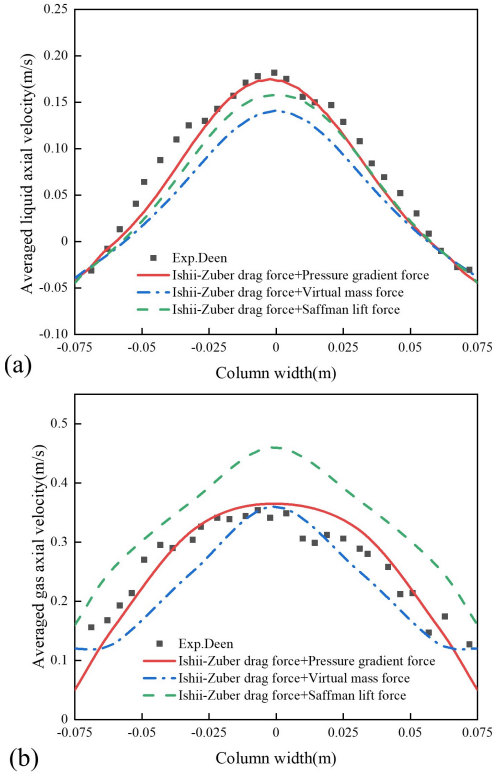

Fig. 5. Effect of different additional interphase forces: (a) time-averaged axial liquid velocity at the height of 0.25m. (b) time-averaged axial gas velocity at the height of 0.25 m.

forces based on the Ishii-Zuber drag model are discussed in the next section.

4.2 Effect of additional force

Based on the results reported in the above sections, the pressure gradient force, virtual mass force and Saffman lift force are introduced to investigate the effect of the different single additional interphase forces. Figure 5(a) compares the mean axial liquid

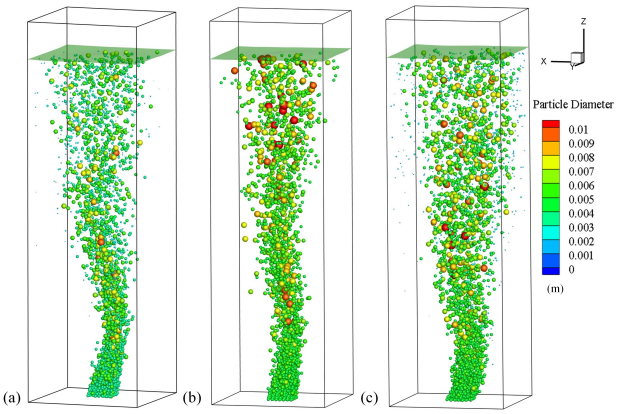

Fig. 6. Instant snapshots of the bubble plume and gas–liquid interface for tested additional interphase forces: (a) pressure gradient force (b) virtual mass force (c) Saffman lift force.

velocity profiles among different single additional interphase forces and the experimental data. The liquid velocity simulated with the pressure gradient force satisfactorily agrees with that of the experiment result, while other additional interphase forces under-estimate the velocity. Comparison of the mean axial gas velocity profiles among different additional interphase forces and the experimental data is shown in Fig. 5(b). Compared with the results that only consider Ishii-Zuber drag model, the introduction of pressure gradient force reduces the mean velocity of the gas and is closer to experiment result. There is a bottom-up pressure gradient in the flow field, and the direction of the pressure gradient force acting on bubbles is opposite to the pressure gradient. Therefore, the pressure gradient force hinders the rise of the bubble, which leads to the decrease of gas velocity. The virtual mass force decelerates the discrete phase, which is responsible for the lower gas velocity compared with that of the experimental data. The simulation result of virtual mass force has a wider diameter distribution compared to other two simulation results in terms of the bubble diameter distribution, as shown in Fig. 7. The maximum diameter of bubble is 13 mm and the peak percentage of bubble diameter is observed at 4mm. The number of bubbles with diameter less than 2mm is greatly reduced, which indicates that the bubbles are more difficult to break up when considering the virtual mass force. On the contrary, under Saffman lift force, the distribution of bubble plume is more homogeneous since Saffman lift is proportional to the velocity gradient. In general, the velocity gradient in the mainstream region is much smaller than the boundary region, thus the force is more remarkable than the boundary region. The direction of Saffman lift force acting on the bubble points at the wall. Due to the velocity gradient between mainstream region and boundary region, the distribution of bubble is more homogeneous which can be found from the Fig. 7. Meanwhile, there are more small bubbles visible as illustrated in Fig. 6(c), the maximum diameter of bubble is 11.5 mm, and the number of 2mm bubble diameter

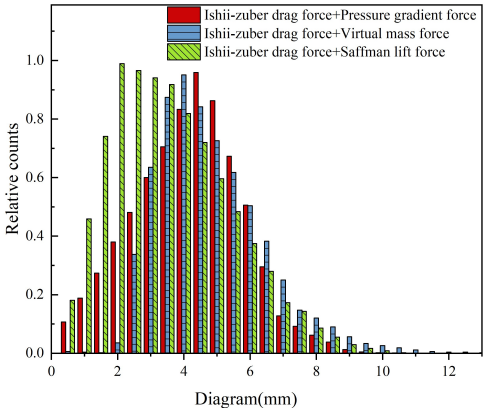

Fig. 7. Overall bubble size distribution for tested additional interphase forces.

distribution is the peak value. Compared with other two simulation results in this section, it contains more bubbles whose diameter is less than 2 mm. With the increase of gas velocity, the turbulence level of liquid phase is more significant, which leads to the bubble break-up and the increase of small bubbles. In summary, the employment of both pressure gradient force and Ishii-Zuber drag model produces better agreement with experimental data for velocity profiles.

The bubble plume oscillation period (POP) can be monitored by analyzing the period of the horizontal velocity. Figure 8 shows the horizontal velocity fluctuation of the bubble plume at point A under different interphase forces overtime. The horizontal fluctuation shows a little irregular. Velocity fluctuations may fluctuate with a large amplitude for a while and then continue to fluctuate at a relatively small amplitude for another while. Typical cycles and periods T are marked in Fig. 8 Compared with the POP under different interphase forces, it can be found that pressure gradient force leads to a longer POP than other two forces, and the POP under the Saffman lift force is the shortest.

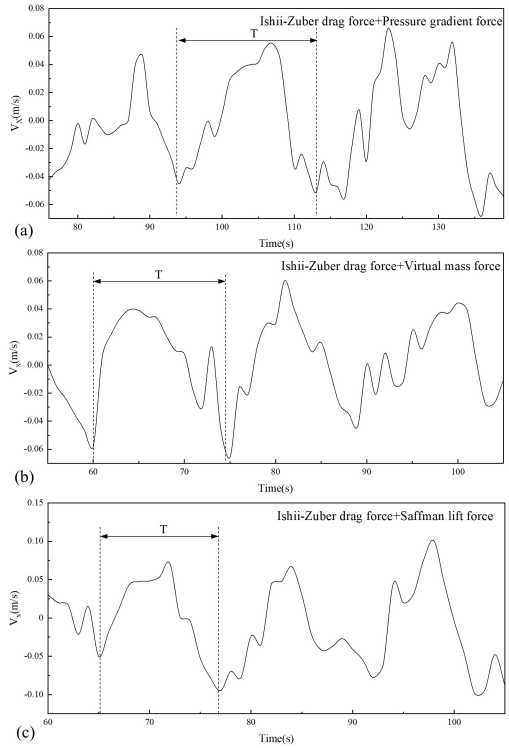

Fig. 8. Time history of the horizontal liquid velocity fluctuation for different additional forces at the height of 0.25 m in the center of the column: (a) pressure gradient force (b) virtual mass force (c) Saffman lift force.

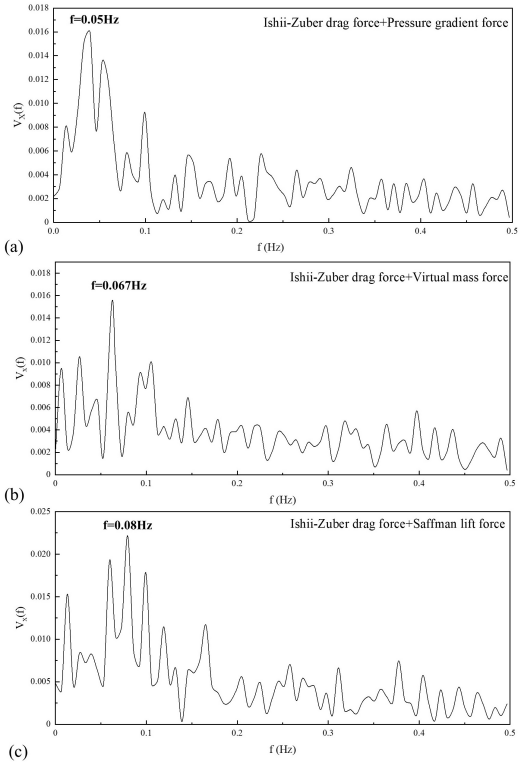

Fig. 9. Amplitude spectrum of horizontal liquid velocity fluctuation for different additional forces at the height of 0.25 m in the center of the column: (a) pressure gradient force (b) virtual mass force (c) Saffman lift force.

A more detailed quantitative analysis of the POP can be investigated by the frequency spectrum of the horizontal velocity fluctuation. Figure 9 plots the horizontal velocity fluctuation, by applying a fast Fourier transformation to the to the simulation time series. The addition of different interphase forces leads to more complex interphase interactions, which makes the velocity fluctuation more irregular. As illustrated in Fig. 9, the frequency of the maximum amplitude of pressure gradient force is 0.05Hz; the frequency of the maximum amplitude of virtual mass force is 0.067Hz; the frequency of the maximum amplitude of Saffman lift force is 0.08Hz. They are corresponding to the marked fluctuation whose periods are about 20s, 15s, 12.5s as seen in Fig. 8. As the Saffman lift force consider, it can be found that several large values of amplitude appear in the frequency spectrum, the fluctuation is much more irregular.

4.3 Effect of multi-interphase forces

As illustrated in Fig. 10., the liquid and gas velocities are under-estimated under the combined effect of pressure gradient force and virtual mass force. Compared with the results that consider only the drag model or pressure gradient force, the addition of virtual mass reduces the velocity of the gas further. It is indicated that the combined effect of pressure gradient force and virtual mass force imposes stronger resistance on the rising of bubble in the flow field. The combined effect of pressure gradient force and Saffman lift force results in an over-prediction of the gas velocity. The discrepancy from experimental data considering the pressure gradient force and the Saffman lift force is less than that only considers the Saffman lift force. Figure 11 shows the flow pattern using different combinations of interphase forces, it is found that the consideration of pressure gradient force and virtual mass force predicts more large bubbles.

Compared with Fig. 7, Fig. 12 shows that both the largest diameter of bubbles and the number of bubbles with diameters more than 4 mm decrease slightly. Furthermore, it is found that the number of bubbles with diameters less than 2 mm decreases due to the addition of the pressure gradient force.

The effect of pressure gradient force and virtual mass force weakens the bubbles coalescence slightly. Similarly, the effect of pressure gradient force and Saffman lift force on bubbles reduces break-up frequency of bubbles than that only considers Saffman lift force.

Figure 13 shows the horizontal velocity fluctuation under different combinations of multi-interphase forces over time. As we can see in the figure, the velocity fluctuations are disordered and periods are not obvious compared with the results in Fig. 8,

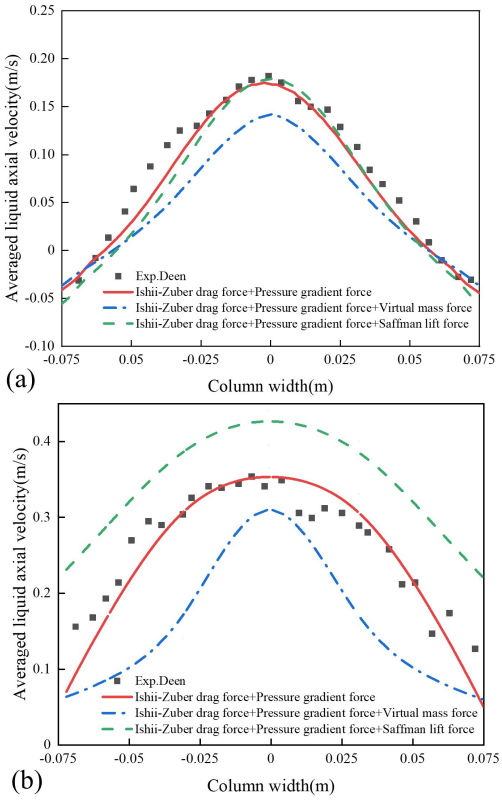

Fig. 10. Effect of different multi-interphase force: (a) time-averaged axial liquid velocity at the height of 0.25m. (b) time-averaged axial liquid velocity at the height of 0.25 m.

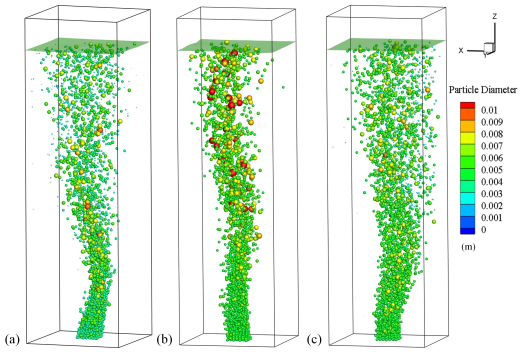

Fig. 11. Instant snapshots of the bubble plume for multi-interphase forces: (a) pressure gradient force (b) pressure gradient force and virtual mass force (c) pressure gradient force and Saffman lift force.

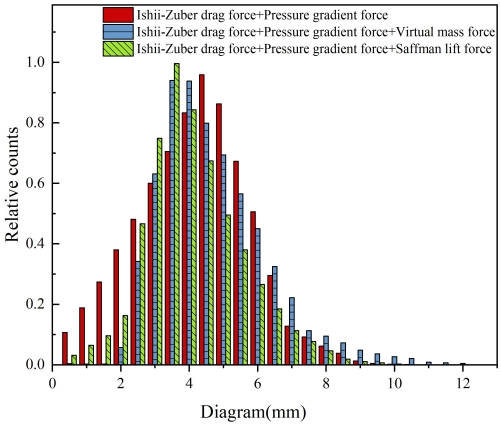

Fig. 12. Overall bubble size distribution for different combinations of multi-interphase forces.

which considers the drag force and one additional force.

Figure 14 plots the amplitude spectrums of the horizontal liquid velocity fluctuation. There are some dominant frequencies between 0 and 0.1 Hz with large amplitude as seen in the figure, which is more in Fig. 14(b). This is probably because of the bubbles oscillate in an irregular and chaotic manner. The results indicate that the combined action of the interphase forces leads to a more complicated interaction between bubble and liquid, which makes the periodic behavior of the bubble plume disappeared.

4.4 Transient flow patterns

In this section, the simulation with coupled pressure gradient force and Ishii-Zuber drag model is conducted to investigate the transient behaviors of gas-liquid flow. The bubble plume and the gas–liquid interface at different times are shown in Fig. 15. The bubble plume is found to oscillate periodically from left to right. The vector field of liquid velocity in Fig. 15(b) shows that the circulation of the liquid phase occurs in the bubble column. Bubbles drive the liquid phase upward while rising, and the downward flow of the liquid phase occurs near the side wall. The surrounding liquid is entrained into the bubble plume continuously and pushes the incoming gas to the center of the bubble column. Vortices formed around the two side walls push the gas along different radial directions to produce the bubble plume oscillation. The bubble plume deviates from the center of the bubble tower and begins to swing due to the asymmetry of the vortex. The plume section is expanding. A lateral flow layer with a velocity gradient appears as bubble plume reach the liquid surface.

5. CONCLUSION

A multi-scale mathematical model based on combined VOF and DBM has been proposed. An Euler-Lagrange method is used to simulate the gas-liquid flow which is widely found in industrial processes. The bubble behavior and dynamics of the gas-liquid interface are well revealed. The dispersed bubble behaviors are investigated by tracking the trajectory of each bubble, and the effect of interphase forces on the gas-liquid flow pattern is

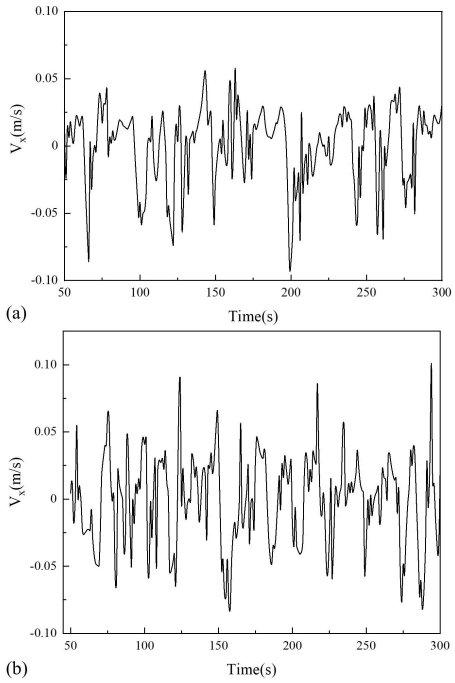

Fig. 13. Time history of the horizontal liquid velocity fluctuation for multi-interphase forces at the height of 0.25 m in the center of the column: (a) pressure gradient force and virtual mass force (b) pressure gradient force and Saffman lift force.

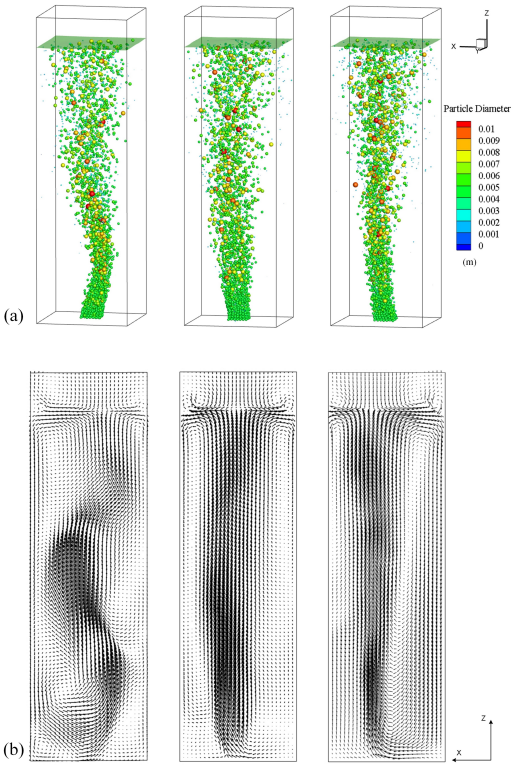

Fig. 15. Instant snapshots on the mid-depth plane at t=255 s, 263 s and 272 s: (a) bubble plume and gas-liquid interface (b) liquid velocity vectors.

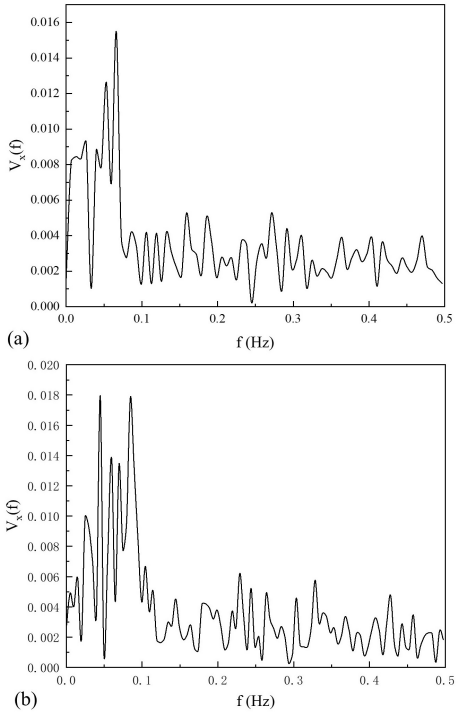

Fig. 14. Amplitude spectrum of horizontal liquid velocity fluctuation for multi-interphase forces at the height of 0.25 m in the center of the column: (a) pressure gradient force and virtual mass force (b) pressure gradient force and Saffman lift force.

evaluated. The hybrid model is verified by the PIV results of Deen *et al.* (2000). Conclusions can be drawn as follows:

-The numerical results of bubble flow patterns and velocity profiles are in good agreement with the measured data, indicating that the application of this multi-scale mathematical model can reasonably predict the gas-liquid two-phase flow.

-For drag closures, the Ishii-Zuber drag model is proven better than the spherical model and the Grace model. The bubble diameter distribution under the Ishii-Zuber model follows a normal distribution approximately. The Grace model promotes the coalescence and breakup of bubbles. On the contrary, the spherical model inhibits the coalescence and breakup of bubbles. It is found that considering both the Ishii-Zuber drag model and the pressure gradient force can predict the liquid and bubble velocity quite well.

-The virtual mass force decelerates discrete phase and bubbles are more concentrated. In addition, weakens bubble breakup. The Saffman lift force increases the velocity of the discrete phase and the turbulence of liquid phase is more significant, which strengthens bubble breakup.

-The pressure gradient force leads to a longer POP than the virtual mass force and the Saffman lift force, the POP under the Saffman lift force is the shortest. The combined action of the interphase forces makes the velocity fluctuations irregularly.

ACKNOWLEDGEMENTS

The authors are grateful to the support by the National Natural Science Foundation of China (Grant No. 51906223, No. 52006197, No. U1709209), the National Science Foundation of Zhejiang Province (Grant No. LQ21E060012, LR20E090001), the Key Research and Development Program of Zhejiang Province (Grant No. 2020C01027) and the Top-notch Talent Support Program of Zhejiang Province (No. 2019R51002).

REFERENCES

Bokkers, G. A., J. A. Laverman and M. V. S Annaland (2006). Modelling of large-scale dense gas–solid bubbling fluidised beds using a novel discrete bubble model. *Chemical Engineering Science* 61(17), 5290-5302.

Brackbill, J. U., D. B. Kothe and C. Zemach (1992). A continuum method for modeling surface tension. *Journal of Computational Physics* 100(2), 335–354.

Chahed, J., V. Roig and L. Masbernat (2003). Eulerian–Eulerian two-fluid model for turbulent gas–liquid bubbly flows. *International Journal of Multipahse Flow* 29, 23-49.

Clift, G. and W. Bubbles (1978). Drops, and Particles. Technical Report. Academic Press.

Cloete, S. W. P., J. J. Eksteen and S. M. Bradshaw (2013). A numerical modelling investigation into design variables influencing mixing efficiency in full scale gas stirred ladles. *Minerals Engineering* 46-47, 16-24.

Darmana, D., N. G. Deen and J. A. M. Kuipers (2006). Parallelization of an Euler–Lagrange model using mixed domain decomposition and a mirror domain technique: Application to dispersed gas–liquid two-phase flow. *Journal of Computational Physics* 220 (1), 216–248.

Deen, N.G., B. H. Hjertager and T. Solberg (2000). Comparison of PIV and LDA Measurement Methods Applied to the Gas-Liquid Flow in a Bubble Column. Proc. 10th Intl Symp. on Appl. of Laser Techniques to Fluid Mech, Lisbon, Portugal.

Deen, N. G., T. Solberg and B. H. Hjertager (2001). Large Eddy simulation of the gas–liquid flow in a square cross-sectioned bubble column. *Chemical Engineering Science* 56, 6341–6349.

Delnoij, E., F. A. Lammers, J. A. M. Kuipers and W. P. M. V. Swaaij (1997). Dynamic simulation of dispersed gas-liquid two-phase flow using a discrete bubble model. *Chemical Engineering Science* 52(9), 1429-1458.

Gosman, A. D. and E. Ioannides (1983). Aspects of computer simulation of liquid-fuelled combustors. *Journal of Energy Chemistry* 7(6), 482–490.

Hirt, C. W. and B. D. Nichols (1981). Volume of fluid (VOF) method for the dynamics of free boundaries. *Journal of Computational Physic* 39, 201-225.

Hoomans, B. P. B., J. A. M. Kuipers, W. J. Briels and W. P. M. V. Swaaij (1996). Discrete particle simulation of bubble and slug formation in a two-dimensional gas-fluidised bed: A hard-sphere approach. *Chemical Engineering Science* 51, 99.

Ishii, M. and N. Zuber (1979). Drag Coefficient and Relative Velocity in Bubbly, Droplet or Particulate Flows. *AIChE Journal* 25, 843-855.

Jain, D., J. A. M. Kuipers and N. G. Deen (2014). Numerical study of coalescence and breakup in a bubble column using a hybrid volume of fluid and discrete bubble model approach. *Chemical Engineering Science* 119, 134-146.

Jiang, X., N. Yang and B. Yang (2016). Computational fluid dynamics simulation of hydrodynamics in the riser of an external loop airlift reactor. *Particuology* 27, 95–101.

Li, A. and G. Ahmadi (1992). Dispersion and Deposition of Spherical Particles from Point Sources in a Turbulent Channel Flow. *Aerosol Science and Technology* 16, 209-226.

Li, L. and B. Li (2018). Implementation and validation of a volume-of-fluid and discrete-element-method combined solver in OpenFOAM. *Particuology* 39, 109-115.

Li, L., B. Li and Z. Liu (2017). Modeling of Gas-Steel-Slag Three-Phase Flow in Ladle Metallurgy: Part II. Multi-scale Mathematical Model. *ISIJ International* 57(11), 1980-1989.

Li, L., X. Li, Z. Zhu and B. Li (2020). Numerical modeling of multiphase flow in gas stirred ladles: From a multiscale point of view. *Powder Technology* 373, 14-25.

Liu, J., C. Zhu, T. Fu and Y. Ma (2014). Systematic Study on the Coalescence and Breakup Behaviors of Multiple Parallel Bubbles Rising in Power-law Fluid. *Industrial & Engineering Chemistry Research* 53, 4850–4860.

Liu, M. and Z. Hu (2004). Studies on the hydrodynamics of chaotic bubbling in a gas–liquid bubble column with a single nozzle. *Chemical Engineering & Technology* 27, 537–547.

Ma, D., M. Liu, Y. Zu and C. Tang (2012). Two-dimensional volume of fluid simulation studies onsingle bubble formation and dynamics in bubble columns. *Chemical Engineering Science* 72, 61–77.

Matiazzo, T., R. K. Decker, J. C. S. C. Bastos, M. K. Silva and H. F. Meier (2020). Investigation of Breakup and Coalescence Models for Churn-Turbulent Gas-Liquid Bubble Columns.

Journal of Applied Fluid Mechanics 13, 737-751.

Menter, F. R. (1994). Two-equation eddy-viscosity turbulence models for engineering applications. *Aiaa Journal* 32(8), 1598-1605.

Morsi, S. A. and A. J. Alexander (1972). An Investigation of Particle Trajectories in Two-Phase Flow Systems. *Journal of Fluid Mechanics* 55(2), 193–208.

Olsen, J. E. and P. Skjetne (2016). Modelling of underwater bubble plumes and gas dissolution with an Eulerian-Lagrangian CFD model. *Applied Ocean Research* 59, 193-200.

O'Rourke, P. J (1981). *Collective Drop Effects on Vaporizing Liquid Sprays*, Ph.D. Thesis, Mechanical and Aerospace Engineering, Princeton University, USA.

Passalacqua, A. and R. O. Fox (2011). Implementation of an iterative solution procedure for multi-fluid gas–particle flow models on unstructured grids. *Powder Technology* 213, 174-187.

Pfleger, D., S. Gomes, N. Gilbert and H. G. Wagner (1999). Hydrodynamic simulations of laboratory scale bubble columns fundamental studies of the Eulerian–Eulerian modelling approach. *Chemical Engineering Science* 54, 5091-5099.

Saffman, P. G. (1965). The Lift on a Small Sphere in a Slow Shear Flow. *Journal of Fluid Mechanics* 22, 385–400.

Bourloutski E. and Sommerfeld M. (2004). Euler/Lagrange Calculations of Gas-Liquid-Solid-Flows in Bubble Columns with Phase Interaction. *In: Sommerfeld M. (eds) Bubbly Flows. Heat and Mass Transfer. Springer, Berlin, Heidelberg*.

van den Hengel, E. I. V., N. G. Deen and J. A. M. Kuipers (2005). Application of Coalescence and Breakup Models in a Discrete Bubble Model for Bubble Columns. *Industrial & Engineering Chemistry Research* 44(14), 5233-5245.

Wang, T. and J. Wang (2007). Numerical simulations of gas-liquid mass transfer in bubble columns with a CFD-PBM coupled model. *Chemical Engineering Science* 62, 7107–7118.

Xu, Y., M. Liu and C. Tang (2013). Three-dimensional CFD-VOF-DPM simulations of effects of low-holdup particles on single-nozzle bubbling behavior in gas-liquid-solid systems. *Chemical Engineering Journal* 222, 292–306.

Zhang, Y., M. Liu, Y. Xu and C. Tang (2012). Three-dimensional volume of fluid simulations on bubble formation and dynamics in bubble columns. *Chemical Engineering Science* 73, 55–78.

Zhou, L. (2010). Advances in studies on two-phase turbulence in dispersed multiphase flows. *International Journal of Multipahse Flow* 36, 100-108.